International Journal of Heat and Mass Transfer 53 (2010) 4152–4167

Contents lists available at ScienceDirect

International Journal of Heat and Mass Transfer

journal homepage: www.elsevier.com/locate/ijhmt

Two-dimensional unsteady forced convection heat transfer in power-law fluids from a cylinder

Vijaya K. Patnana, Ram P. Bharti [1], Raj P. Chhabra *

Department of Chemical Engineering, Indian Institute of Technology, Kanpur 208016, UP, India

ARTICLE INFO

Article history:
Received 2 May 2009
Received in revised form 9 November 2009
Accepted 16 February 2010
Available online 10 June 2010

Keywords:
Power-law fluids
Reynolds number
Prandtl number
Nusselt number
Circular cylinder
Unsteady forced convection heat transfer

ABSTRACT

Forced convection heat transfer characteristics of a cylinder (maintained at a constant temperature) immersed in a streaming power-law fluids have been studied numerically in the two-dimensional (2-D), unsteady flow regime. The governing equations, namely, continuity, momentum and thermal energy, have been solved using a finite volume method based solver (FLUENT 6.3) over wide ranges of conditions (power law index, $0.4 \leqslant n \leqslant 1.8$; Reynolds number, $40 \leqslant Re \leqslant 140$; Prandtl number, $1 \leqslant Pr \leqslant 100$). In particular, extensive numerical results elucidating the influence of Reynolds number, Prandtl number and power-law index on the isotherm patterns, local and average Nusselt numbers and their evolution with time are discussed in detail. Over the ranges of conditions considered herein, the nature of flow is fully periodic in time. The heat transfer characteristics are seen to be influenced in an intricate manner by the value of the Reynolds number (Re), Prandtl number (Pr) and the power-law index (n). Depending upon the value of the power-law index (n), though the flow transits from being steady to unsteady somewhere in the range $\sim 33 < Re < 50$, the fully periodic behavior is seen only beyond the critical value of the Reynolds number (Re). As expected, the average Nusselt number increases with an increase in the values of Reynolds and/or Prandtl numbers, irrespective of the value of the flow behavior index. A strong influence of the power-law index on both local and time-averaged Nusselt numbers was observed. Broadly, all else being equal, shear-thinning behavior ($n < 1$) promotes heat transfer whereas shear-thickening behavior ($n > 1$) impedes it. Furthermore, this effect is much more pronounced in shear-thinning fluids than that in shear-thickening fluids.

1. Introduction

The flow past a circular cylinder represents a classical problem in fluid mechanics and has thus received considerable attention over the past 50 years or so. This flow also denotes an idealization of many industrial applications such as the flow in tubular and pin-type heat exchangers, in the use of thin wires as measuring probes, in thermal processing of food particles, etc. Consequently, over the years, a significant body of knowledge has accrued on various aspects including flow regimes and their transitions, gross engineering parameters like hydrodynamic forces (lift and drag coefficients) exerted on a cylinder immersed in moving fluids, rates of heat and mass transfer and detailed structures of the flow field like wake phenomenon, vortex shedding, isotherm patterns, etc. Undoubtedly, the field has attained a level of maturity, as far as the behavior of Newtonian fluids is concerned. Excellent reviews and survey articles, even books exclusively devoted to the flow over a single cylinder are now available [1–3]. Suffice it to add here that even for Newtonian fluids, the momentum characteristics have been studied much more thoroughly than the corresponding heat/mass transfer problems for this flow configuration.

On the other hand, many so-called "structured" substances of multi-phase nature and/or of high molecular weight encountered in industrial practice (pulp and paper suspensions, food, polymer melts and solutions, foams, micellar solutions, etc.) display shear-dependent flow behavior [4]. Owing to their high viscosity levels, it is common to encounter laminar flow conditions in the processing of these materials. Admittedly, many non-Newtonian fluids, notably, polymeric systems also display visco-elastic behavior; the available scant literature both for the creeping flow past a single cylinder and over a periodic array of cylinders seems to suggest the visco-elastic effects to be minor in this flow configuration [5]. Furthermore, currently available visco-elastic simulations examine the role of visco-elasticity in the absence of shear-thinning behavior in the limit of zero Reynolds number (creeping flow) and under these conditions, the elasticity effect is predicted to be small. On the other hand, the test fluids used in the few experimental studies available displays both shear-dependent viscosity and visco-elastic characteristics. Therefore, it is not only unfair to

* Corresponding author. Tel.: +91 512 259 7393; fax: +91 512 259 0104.
E-mail address: chhabra@iitk.ac.in (R.P. Chhabra).
[1] Present address: Department of Chemical Engineering, Indian Institute of Technology, Roorkee 247667, Uttrakhand, India.

0017-9310/$ - see front matter © 2010 Elsevier Ltd. All rights reserved.
doi:10.1016/j.ijheatmasstransfer.2010.05.038

Nomenclature

c_p	specific heat of the fluid, J/kg K
D	diameter of the cylinder, m
h	convective heat transfer coefficient, W/m^2 K
H	height of the computational domain, m
I_2	second invariant of the rate of the strain tensor, s^{-2}
L	length of the computational domain, m
L_u	upstream length, i.e., the distance from the inlet boundary to center of the cylinder, m
L_d	downstream length, i.e., distance from center of the cylinder to outflow boundary, m
m	power-law consistency index, Pa s^n
n	power-law flow behavior index, dimensionless
Nu	time-averaged surface averaged Nusselt number, dimensionless
Nu^N	normalized average Nusselt number using the corresponding Newtonian value, [=Nu(non-Newtonian)/Nu(newtonian)], dimensionless
$Nu(\theta)$	Local Nusselt number (Nu_{Local}) over the surface of the cylinder, dimensionless
p	pressure, Pa
p_o	free stream pressure, Pa
Pr	Prandtl number, dimensionless
Re	approach Reynolds number, dimensionless
t	time, s
T	time period, s
T	temperature, K
T_o	temperature of the fluid at the inlet, K
T_w	temperature of the surface of the cylinder, K
U_o	uniform inlet velocity of the fluid, m/s
U_x, U_y	x-and y-components of the velocity, m/s
x,y	stream-wise and transverse coordinates, m

Greek symbols

η	viscosity, Pa s
θ	angular displacement from the front stagnation ($\theta = 0$), degrees
ρ	density of the fluid, kg/m^3
τ	shear stress, Pa
τ_{xx}, τ_{xy}	x-and y-components of the extra stress tensor, Pa

Subscript

Local point value

compare these experiments with numerical predictions, but it is also not obvious whether the significant deviations seen from the Newtonian kinematics are due to their shear-dependent viscosity or visco-elasticity or due to a combination of both [5]. Therefore, it seems reasonable to begin with the analysis of purely viscous power-law type fluids as long as the power-law constants are evaluated in the shear-rate range appropriate for the flow over a cylinder, and the level of complexity can then be built up gradually to accommodate other non-Newtonian characteristics such as yield stress, visco-elasticity, etc.

As far as known to us, there has been no prior study on the convective heat transfer from a heated circular cylinder to incompressible power-law liquids in the two-dimensional periodic (unsteady) flow regime. This constitutes the main objective of this work. At the outset, it is, however, useful to briefly recount the available limited work on the flow of Newtonian fluids in the unsteady flow regime and of power-law fluids past a cylinder to facilitate the subsequent presentation of the new results on heat transfer in the time-dependent periodic flow regime.

2. Previous work

It is instructive to recapitulate the flow regimes observed for the flow of Newtonian fluids over a long cylinder oriented normal to the direction of flow. It is now readily agreed that, for an unconfined flow, the first signature of flow separation occurs at about Reynolds number, $Re \sim 4$–5. As the Reynolds number, Re, is gradually incremented, the two symmetric vortices grow in size up to about Reynolds number, $Re \sim 46$–47 [6,7] (albeit values ranging from 45 to 50 have been reported in the literature, e.g., see [1,2]) when the flow becomes asymmetric about the mid-plane and this is followed by vortex shedding, thereby leading to the periodic (time-dependent) flow regime, albeit the flow is still two-dimensional (2-D). This flow regime persists up to about $Re \sim 188.5 \pm 1$ [8] (though values ranging from ~170 to ~190 have been cited in the literature, e.g., see [1,2]) and beyond this value, the flow ultimately transits to three-dimensional (3-D) in character. Naturally, such changes in the detailed kinematics also manifest at macroscopic level via the different scalings of the drag and lift coefficients, Nusselt number, etc. with the Reynolds number. Additional complications arise from the presence of confining walls, entry velocity profiles, etc. It is, therefore, impossible to develop a single sound theoretical framework to estimate the values of the engineering parameters spanning all flow regimes [1,9]. While numerous studies delineating the fluid mechanical aspects in the laminar vortex shedding regime are available [1,9], only scant literature is available on the corresponding convective heat transfer problem even in Newtonian fluids. Since a detailed review of the pertinent literature up to 1996 is available elsewhere [10], only the key points and/or the subsequent studies are included here.

Most studies on heat transfer relate to the flow of air and are thus restricted to the single value of the Prandtl number, $Pr = 0.71$. Only very recently, the effect of a 100-fold variation in the value of Prandtl number (Pr) has been investigated numerically in the steady flow regime up to Reynolds number, $Re = 40$ [11]. Similarly, while the flow is known to be time-dependent beyond $Re \geqslant 46$–47, many investigators have sought steady state solutions to the governing equations, e.g., see [10,12], and obviously, it is difficult to justify this assumption for Reynolds number, $Re > \sim 47$. Therefore, there have been relatively a few time-dependent studies for convective heat transfer from a heated cylinder even in Newtonian fluids. For instance, Karniadakis [13] presented limited results on Nusselt number for a cylinder in air up to Reynolds number (Re) of 200 and found these to be in good agreement with the experimental results available in the literature. Similarly, Cheng et al. [14] studied the so-called lock-on effect on convective heat transfer from a transversely oscillating circular cylinder. They considered two values of the Prandtl number (Pr), corresponding to air and water, i.e., ~0.7 and 7, respectively. For the case of a non-oscillating cylinder, they reported time-averaged values of the drag coefficient and heat transfer up to $Re = 200$ which were shown to be in line with the other pertinent studies. Subsequently, Mahfouz and Badr [15] have examined the influence of rotational oscillation of a cylinder on forced convection heat transfer in air. In the limiting case of a fixed cylinder, they also demonstrated the periodic-variation in Nusselt number at three values of the Reynolds number, $Re = 80$,100 and 200. Their time averaged values of Nusselt number are also consistent with the prior numerical and experimental

values. In an extensive study, Lange et al. [16] studied numerically heat transfer from a cylinder to air in the range of Reynolds number as $Re \leqslant 200$. In particular, they tried to ascertain the effect of temperature-dependent properties on heat transfer. Similarly, Baranyi [17] has also numerically studied heat transfer from a heated cylinder to air in the range of Reynolds number as $50 \leqslant Re \leqslant 180$ over which the flow can be treated as two-dimensional (2-D). He reported detailed results on momentum and heat transfer characteristics. Thus, in summary, only limited numerical studies are available on heat transfer from a cylinder in the time-dependent regime even in Newtonian media, and most of these relate to air. Therefore, very little is known about the effect of Prandtl number (Pr) on heat transfer from a cylinder in the time-dependent regime.

In contrast, the corresponding literature on the flow of power-law fluids over a cylinder is not only of recent vintage, but is also less extensive and is restricted only to the steady flow regime. Furthermore, early studies [18–22] invariably assumed the identical flow regimes to exist as that for Newtonian fluids. Thus, for instance, D'Alessio and Pascal [18], Chhabra et al.[19], Soares et al. [20], Bharti et al. [21,22], etc., all reported the values of flow and heat transfer parameters over wide ranges of power-law index (n), Prandtl number (Pr) and up to about $Re = 40$ by assuming the flow to be steady. It is now readily acknowledged [23] that the wake formation is delayed to about $Re \sim 11$–12 in shear-thinning ($n < 1$) fluids and it occurs at as low a value as $Re \sim 0.3$ in shear-thickening ($n > 1$) fluids. Similarly, the steady flow regime ends at $Re \sim 33$–35 in highly shear-thickening ($n > 1$) fluids [23]. This clearly casts some doubts about the reliability of the results based on the assumption of the steady flow regime, as also noted above for Newtonian fluids. Notwithstanding this intrinsic limitation, suffice it to add here that reliable results are now available on heat transfer from a cylinder immersed in streaming power-law fluids up to about Prandtl number (Pr) values of 100–200 [20,22]. Similarly, the role of mixed convection has been elucidated recently in the cross-flow and aiding buoyancy configurations and under appropriate conditions, free convection can augment the overall rate of heat transfer by up to 40–45% in shear-thinning ($n < 1$) fluids [24,25]. Thus, a reasonable amount of information is available on convective heat transfer from a cylinder in power-law fluids. By virtue of the steady flow assumption, these results are limited to a maximum value of the Reynolds number, $Re \sim 40$. Some of the other relevant studies include elliptic cylinders in power-law fluids [26,27], confined circular cylinder [28,29], two cylinders in tandem arrangement [30,31], square cylinder in power-law fluids [32–34], albeit the steady flow assumption is implicit in all these studies, with a notable exception of [35,36].

As far as known to us, there has been only one study of vortex-shedding from a cylinder in power-law fluids [37]. The key findings of this work are summarized here. For highly shear-thickening fluids ($n = 1.8$), the unsteady flow was observed at $Re = 40$, and unsteadiness was evident at $Re = 50$ for all values of power-law index (n). As expected, the evolution of the kinematics and vortex shedding phenomenon exhibit complex dependence on the pertinent flow governing parameters in the transition region. For a fixed value of the Reynolds number (Re), the drag coefficient increased whereas both the lift coefficient and Strouhal number decreased as the power-law index (n) was gradually increased, i.e., as the fluid behavior changed from shear-thinning ($n < 1$) to shear-thickening ($n > 1$) via the standard Newtonian ($n = 1$) fluid behavior. For a fixed value of the power-law index (n), the drag coefficient gradually increased with Reynolds number (Re). Undoubtedly, these changes seen in the flow field will directly influence the temperature field in the vicinity of the cylinder and also the overall heat transfer coefficient. However, no such prior study on heat transfer is currently available in the literature.

From the foregoing discussion, it is thus abundantly clear that (i) only limited numerical results are available on heat transfer from a cylinder in Newtonian fluids (mostly air) in the laminar vortex-shedding regime, and (ii) no prior results are available on the time-dependent heat transfer from a cylinder in power law fluids. This work aims to fill these gaps in the literature. In particular, reported herein are extensive numerical results to delineate the role of power law index, Reynolds and Prandtl numbers on the local and averaged heat transfer characteristics in the two-dimensional unsteady flow regime over the following ranges of conditions: Reynolds number ($40 \leqslant Re \leqslant 140$), Prandtl number ($1 \leqslant Pr \leqslant 100$), and power-law index ($0.4 \leqslant n \leqslant 1.8$) thereby including shear-thinning, Newtonian and shear-thickening fluid behaviors.

3. Problem statement and governing equations

Consider the two-dimensional (2-D), unsteady flow of an incompressible power-law liquid streaming with a uniform velocity (U_0) and temperature (T_0) over an infinitely long circular cylinder (of diameter, D) oriented with its long axis normal to the flow, as shown in Fig. 1a. The surface of the cylinder is maintained at a constant wall temperature, T_w ($>T_0$). In order to keep the level of complexity at a tractable level at this stage, the viscous dissipation effects are assumed to be negligible and the thermo-physical properties (heat capacity, thermal conductivity, viscosity and density) of the liquid are assumed to be independent of temperature. While these two assumptions lead to the de-coupling of the momentum and thermal energy equations, these also restrict the applicability of the present results to the situations where the temperature difference between the fluid and cylinder is not too large and for moderate viscosity and/or shearing levels so that the viscous dissipation effects are negligible. In the present simulations, therefore, the temperature difference ΔT ($=T_w - T_0$) is maintained small so that these simplifying assumptions can be justified.

Naturally, it is not possible to mimic truly the unconfined flow condition, it is simulated here by considering the flow in a channel (of height H) with the cylinder placed symmetrically in between the two plane walls with slip boundary conditions (i.e., no dissipation at the walls), as shown schematically in Fig. 1b. The cylinder is placed at an upstream distance of L_u from the inlet boundary and at a distance of L_d (downstream length) from the outflow boundary. The dimensions of the computational domain (Fig. 1b) $L = L_u + L_d$ and height H are taken to be sufficiently large to minimize the end and boundary effects, as discussed in detail in a later section.

The flow and temperature fields are governed by the continuity, momentum and thermal energy equations for this flow, which, in their compact forms are written as follows:

- *Continuity equation:*

$$\nabla \cdot \mathbf{U} = 0 \tag{1}$$

- *Momentum equation:*

$$\rho\left(\frac{\partial \mathbf{U}}{\partial t} + \mathbf{U} \cdot \nabla \mathbf{U} - f\right) - \nabla \cdot \sigma = 0 \tag{2}$$

- *Energy equation:*

$$\rho c_p\left(\frac{\partial T}{\partial t} + \mathbf{U} \cdot \nabla T\right) - k\nabla^2 T = 0 \tag{3}$$

where ρ, $\mathbf{U}$, T, f, c_p, k and σ are the density of the power-law fluid, velocity vector (U_x and U_y components in Cartesian coordinates), temperature, body force, heat capacity, thermal conductivity and

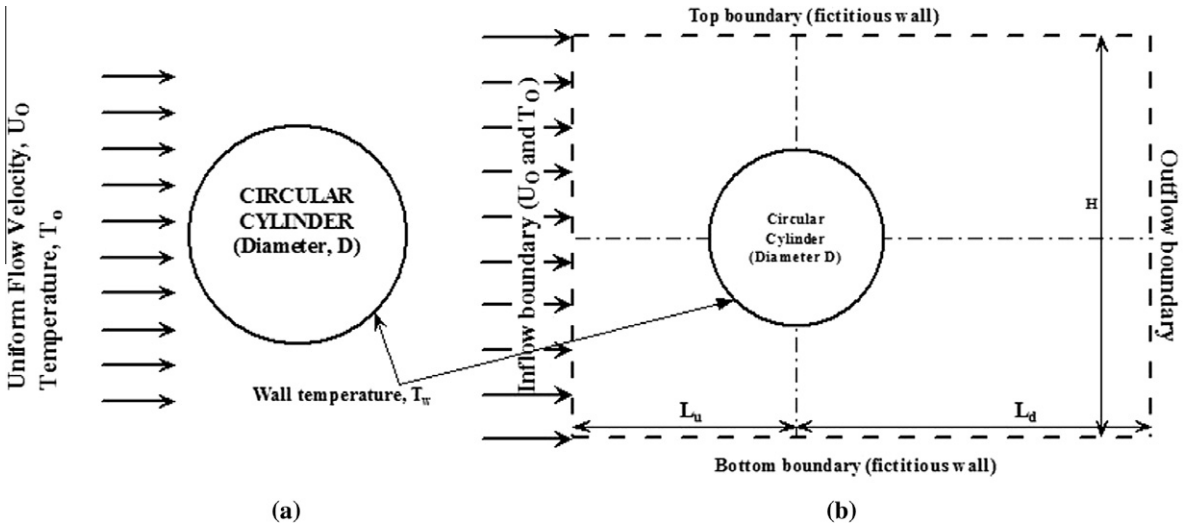

Fig. 1. Schematic representation of (a) a flow over an unconfined cylinder and (b) an approximation of an unconfined flow (uniform velocity, U_o and temperature, T_0) configuration.

the stress tensor, respectively. The stress tensor, sum of the isotropic pressure (p) and the deviatoric stress tensor (τ), is given by

$$\sigma = -pI + \tau \tag{4}$$

For incompressible fluids, the extra stress tensor is related to the rate of deformation tensor as

$$\tau = 2\eta\varepsilon \tag{5}$$

where ε, the components of the rate of strain tensor, are given by

$$\varepsilon = \frac{1}{2}\left[(\nabla \mathbf{U}) + (\nabla \mathbf{U})^T\right] \tag{6}$$

For a power-law fluid, the viscosity (η) is given by

$$\eta = m(I_2/2)^{(n-1)/2} \qquad \text{where} \quad I_2 = 2(\varepsilon : \varepsilon) \tag{7}$$

In Eq. (7), m is the power-law consistency index and n is the power-law index of the fluid ($n < 1$: shear-thinning; $n = 1$: Newtonian; and $n > 1$: shear-thickening) and I_2 is the second invariant of the rate of strain tensor (ε). The components of the rate of strain tensor are related to the velocity components and their derivatives, e.g., see, Ref. [38].

The physically realistic boundary conditions for this flow configuration may be written as follows:

- *At the inlet boundary*: The uniform flow in the x-direction and uniform fluid temperature are imposed at the inlet as.

$$U_x = U_0, \quad U_y = 0 \quad \text{and} \quad T = T_0 \tag{8}$$

- *On the surface of the cylinder*: The standard *no-slip* condition is used and the cylinder is heated so that its surface is maintained at a constant temperature T_w,

$$U_x = 0, \quad U_y = 0 \quad \text{and} \quad T = T_w \tag{9}$$

- *At the exit boundary*: The default outflow boundary condition option in FLUENT (a zero diffusion flux for all flow variables) has been used in this work. This choice implies that the conditions of the outflow plane are extrapolated from within the domain and as such have negligible influence on the upstream flow conditions. The extrapolation procedure used by FLUENT updates the outflow velocity and the pressure in a manner that is consistent with the fully-developed flow assumption, when there is no area change at the outflow boundary. However, the gradients in the cross-stream direction may still exist at the outflow boundary. Also, the use of this condition obviates the need to prescribe a boundary condition for pressure. This is similar to the homogeneous Neumann condition, i.e.,

$$\frac{\partial \phi}{\partial t} + U_0 \frac{\partial \phi}{\partial x} = 0 \quad \text{where} \quad \phi = U_x, U_y \quad \text{and} \quad T \tag{10}$$

- *At the top and bottom boundaries*: Since these are fictitious walls the usual slip flow and adiabatic conditions are imposed, i.e.,

$$\frac{\partial U_x}{\partial y} = 0, \quad U_y = 0 \quad \text{and} \quad \frac{\partial T}{\partial y} = 0 \tag{11}$$

The numerical solution of the governing equations (Eqs. (1)–(3)) in conjunction with the above-noted boundary conditions (Eqs. (8)–(11)) maps the flow domain in terms of the primitive variables, i.e., velocity (U_x and U_y), pressure (p) and temperature (T) fields. These, in turn, are used to deduce the local and global momentum characteristics as outlined below and detailed elsewhere [21,22,26–31]. However, at this stage, it is useful to introduce the definitions of the dimensionless parameters used in the presentation of results.

- The *Reynolds number* (Re) and *Prandtl number* (Pr) for power-law fluids (based on the free stream velocity) are defined as follows:

$$Re = \frac{\rho D^n U_o^{2-n}}{m} \quad \text{and} \quad Pr = \frac{mc_p}{k}\left(\frac{U_o}{D}\right)^{(n-1)} \tag{12}$$

Note that unlike in the case of Newtonian fluids, the Prandtl number (Pr) for a power law fluid depends upon the velocity and diameter of the cylinder, in addition to the thermo-physical properties. However, the Peclet number, Pe (=Re·Pr) is independent of the power-law parameters (m, n).

- The *local Nusselt number*, $Nu(\theta)$ or Nu_{local} on the surface of the cylinder is evaluated using the temperature field as follows:

$$Nu(\theta) = \frac{hD}{k} = -\frac{\partial T}{\partial \boldsymbol{n}_s} \tag{13}$$

where, $\boldsymbol{n}_s$ (the unit vector normal to the surface of the cylinder) is given as

$$\boldsymbol{n}_s = \frac{xe_x + ye_y}{\sqrt{x^2+y^2}} = \boldsymbol{n}_x e_x + \boldsymbol{n}_y e_y \tag{14}$$

where e_x and e_y are the x- and y-components of the unit vector, respectively.

The overall surface average value is obtained by integrating $Nu(\theta)$ over the surface of the cylinder as:

$$Nu = \frac{1}{2\pi}\int_0^{2\pi} Nu(\theta)d\theta \tag{15}$$

It is this value of the average Nusselt number which is frequently needed in process engineering design calculations to estimate the rate of heat transfer from an isothermal cylinder or conversely, to estimate the temperature of the cylinder for a given rate of heat transfer.

Dimensional analysis of the field equations and boundary conditions suggests the average Nusselt number to be a function of the kinematic and dimensionless numbers, i.e., $Nu = f(Re, n, Pr)$, though in view of the periodic nature of the flow, the Nusselt number shows a periodic variation with time (t). This functional relationship is developed in this study.

4. Numerical solution procedure

Since detailed descriptions of the numerical solution procedure are available elsewhere [21–23,25–31,37], only the salient features are recapitulated here. In this study, the field equations have been solved using FLUENT (version 6.3). The unstructured 'quadrilateral' cells of non-uniform grid spacing were generated using the commercial grid tool GAMBIT. The two-dimensional, unsteady, laminar, segregated solver was used to solve the incompressible flow on the collocated grid arrangement. The *second order upwind* scheme has been used to discretize the convective terms in the momentum and thermal energy equations. The semi-implicit method for the pressure linked equations (SIMPLE) scheme was used for solving the pressure-velocity decoupling. The '*constant density*' and '*non-Newtonian power-law*' viscosity models were used. FLUENT solves the system of algebraic equations using the Gauss–Seidel (G–S) point-by-point iterative method in conjunction with the algebraic multi-grid (AMG) method solver. The use of AMG scheme can greatly reduce the number of iterations and thus, the CPU time required to obtain a converged solution, particularly when the model contains a large number of control volumes. Relative convergence criteria of 10^{-8} for the continuity and x- and y-components of the velocity and 10^{-15} for residuals of thermal energy equation were prescribed in this work. Also, the solution is assumed to have converged when there was no change (at least up to fourth decimal place) in the total drag coefficient and the corresponding changes in the value of the lift coefficient are of the order of 10^{-5}–10^{-6} for more than 1000 time steps or when it shows more than 10 constant periodic cycles in time-history of the lift and drag coefficients and surface averaged Nusselt number.

5. Choice of computational parameters

In this work, the effects of Reynolds number (Re), power-law index (n) and Prandtl number (Pr) on the two-dimensional unsteady heat transfer characteristics using the full computational domain (Fig. 1b) are investigated in the following ranges of conditions: Reynolds number (Re = 40, 50, 100, 120 and 140), power-law index (n = 0.4, 0.6, 1, 1.2, 1.4 and 1.8) thereby covering both shear-thinning ($n < 1$) and shear-thickening ($n > 1$) fluid characteristics. The Prandtl number values are chosen as Pr = 1, 10, 50 and 100 so that heat transfer characteristics can be assessed over a wide ranges of fluids. It is appropriate to add here that it is common to encounter industrial fluids (in food and pharmaceutical processing engineering) with the value of Prandtl number (Pr) as large as 100, or even higher [39]. However, in numerical studies, the maximum value of the Prandtl number (Pr) is also restricted by the fact that very fine grids are required near the cylinder owing to the progressive thinning of the thermal boundary layer with increasing Prandtl number (Pr). However, a 100-fold variation in the value of Prandtl number (Pr) covered in this work should provide an adequate guide for delineating the scaling of the Nusselt number (Nu) with Prandtl number (Pr). The ranges of parameters selected here are thus governed, in part, by the typical values encountered in process engineering applications.

Needless to say that the reliability and accuracy of the numerical results is strongly influenced by the choice of numerical parameters, namely, optimal domain and grid sizes and the time step. Similar to our previous study [37], the computational domain in this study is characterized by the values of L_u, L_d and H, the upstream and downstream lengths and height. An excessively large value of these parameters will warrant enormous computational resources and a small value will unduly influence the results and hence a judicious choice is germane to the accuracy of results. Similarly, an optimal grid should be sufficiently fine to adequately capture the flow and temperature fields without being excessively resources intensive. In the numerical simulations of the unsteady flows, the choice of time step ($\Delta t = T/Ns$ where $T = D/U_o$ and Ns are the characteristics time of one periodic oscillation and number of time steps per period, respectively) also plays an important role in obtaining the time accurate solutions of the momentum and energy equations. Based on our previous study, the time step $\Delta t = T/100$ is used in the present investigation. The extent of domain and grid effects on momentum characteristics of unsteady flow of power-law fluids over a cylinder have been discussed in detail in a recent study [37]. Based on our previous experience [19–31], the domain and grids used in the unsteady flow calculations [37] are assumed to be adequate to resolve the heat transfer phenomena with acceptable levels of accuracy within the range of conditions of interest here. Thus, all results reported herein are based on the following choices [37]: the domain size ($L_u = 20D$, $L_d = 80D$ and $H = 90D$) and grid size G_3 which consists of 212323 cells (for more details, see, [37]). Finally, to add further weight to our claim for the accuracy of the results, the numerical results obtained herein have been compared with the literature values in the next section.

6. Results and discussion

Prior to presenting the new results obtained in this work, it is appropriate to validate the solution procedure to ascertain the accuracy and reliability of the results presented herein. This is accomplished by presenting comparisons with the prior results for a few cases.

6.1. Validation of results

Since extensive comparisons for the flow of Newtonian and power-law fluids past a single cylinder and two cylinder system in steady and unsteady flow regimes have been dealt with in detail elsewhere [11,19–31], only the additional limited comparisons for the unsteady heat transfer are presented here in Table 1. An excellent correspondence can be seen to exist between the present and literature values. Sivakumar et al. [23] showed this flow to be steady at Re = 40 for shear-thickening fluids ($n \leqslant 1.4$) and therefore the present values (based on an unsteady solution) are in good agreement with the previous values based on the assumption of steady flow. On the other hand, for highly shear-thickening fluid (n = 1.8),

Table 1
Comparison of the present average Nusselt number ($\overline{Nu}$) values with the literature values for a range of conditions.

Source	$Re = 40$, $Pr = 1$			$Re = 40$, $Pr = 100$		
	$n = 0.6$	$n = 1.0$	$n = 1.8$	$n = 0.6$	$n = 1.0$	$n = 1.8$
Present	4.0775	3.6755	3.2772 ± 0.0001	21.0598	17.9052	16.1327 ± 0.0004
Bharti et al. [27]	4.0545	3.6533	3.2321	20.8647	17.7713	15.4875
Soares et al. [20]	–	3.5700	–	–	–	
						$Re = 100$, $n = 1$, $Pr = 0.71$
Present						5.1529 ± 0.0021
Karniadakis [13]						5.7000
Cheng et al. [14]						4.8584
Mahfouz and Badr [15]						5.3100
Lange et al.[16]						5.128
Baranyi [17]						5.132

Table 2
Comparison between the present values and experimental values of Nusselt number in Newtonian fluids.

Pr	Re	Average Nusselt number (Nu)		
		Ref. [40]	Ref. [41]	Present
0.7	100	5.26	4.62	5.153
10	50	–	9.14	9.18
	100	–	13.28	13.94
	140	–	15.94	16.58
50	50	–	17.41	16.27
	100	–	25.30	24.38
	140	–	30.36	28.82
100	50	–	22.98	21.25
	100	–	33.40	30.90
	140	–	40.07	36.47

the flow transits from being steady to unsteady at about Reynolds number, $Re = 34$–35 and therefore, at $Re = 40$, the flow is likely to be unsteady. In spite of this fact, the time averaged values of the Nusselt number obtained using unsteady and steady state schemes for $n = 1.8$ and $Re = 40$ are close to each other at smaller value of the Prandtl number ($Pr = 1$), but the two values differ by up to

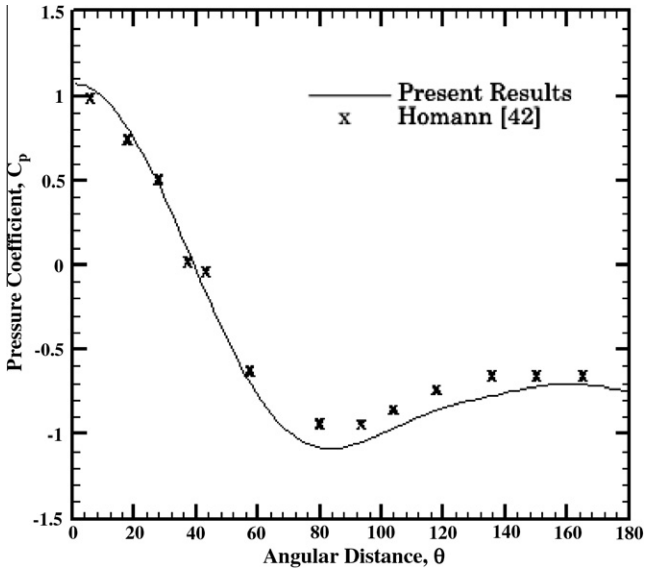

Fig. 2. Comparison between the present predictions of the surface pressure coefficient [$C_p = 2(p-p_0)/(U_0^2)$ where p_0 is the free stream pressure] with experimental data [42] at $Re = 107$.

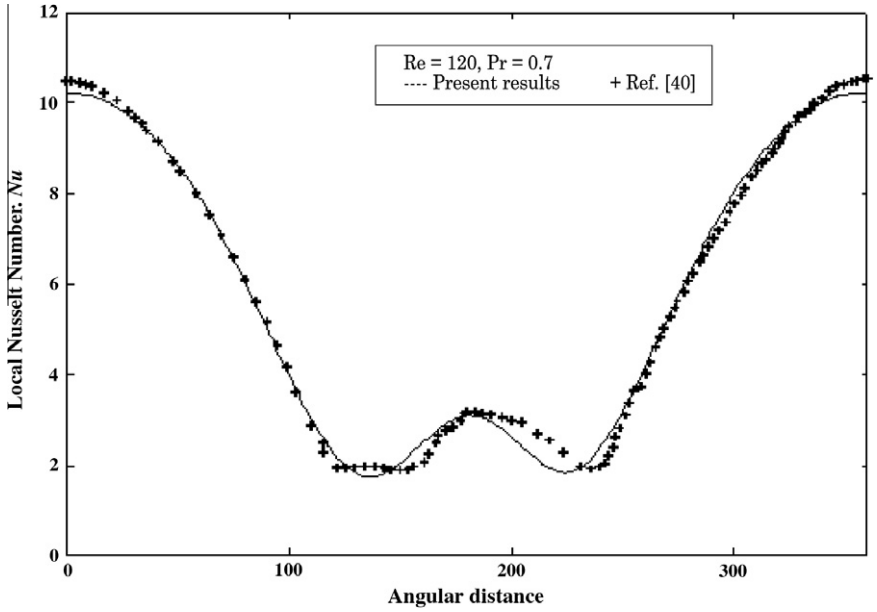

Fig. 3. Comparison between the present predictions of Nusselt number with experimental data [40] at $Re = 120$ and $Pr = 0.7$.

8–9% at $Pr = 100$. This difference is likely to grow further with the increasing values of Reynolds number and/or Prandtl number and/or both. Hence the steady state values will become increasingly less accurate as the Reynolds number (Re) is gradually increased. Next, the present value of the average Nusselt number of 5.1529 for $Re = 100$ and $Pr = 0.71$ compares favorably with the numerical studies of Mahfouz and Badr [15], Karniadakis [13], Cheng et al. [14] and of Baranyi [17]. It is worthwhile to re-iterate here that the discrepancies of this magnitude are not at all uncommon in such numerical studies. Finally, included in Table 2 is a comparison between the present numerical results and the experimental data available in the literature. For air ($Pr = 0.7$), the present value of

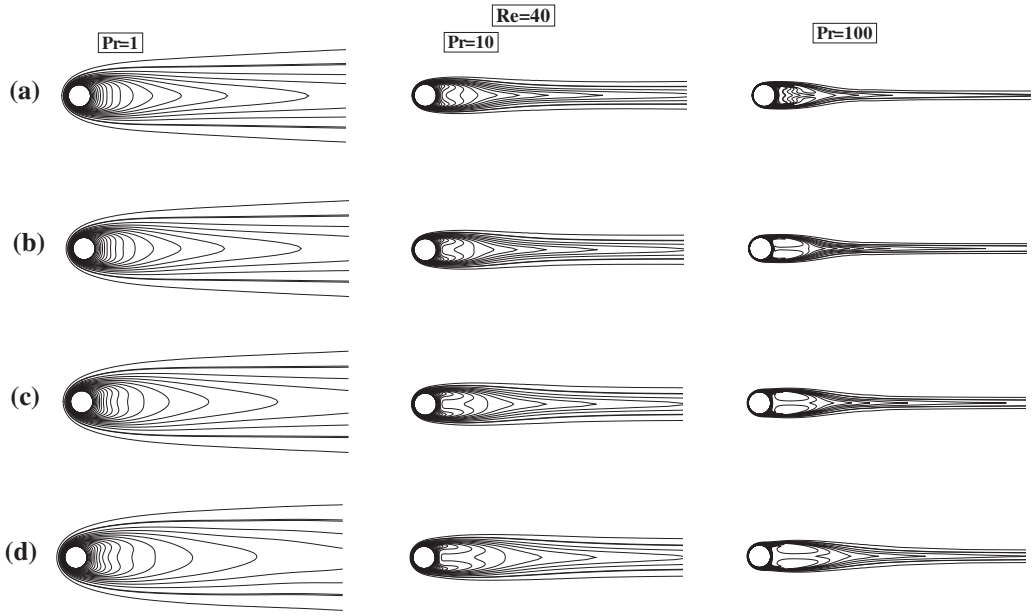

Fig. 4. Isotherm profiles at $Re = 40$ and $Pr = 1$, 10 and 100 and for power-law index: (a) $n = 0.4$, (b) $n = 0.6$, (c) $n = 1$ and (d) $n = 1.4$ for a cylinder in cross-flow.

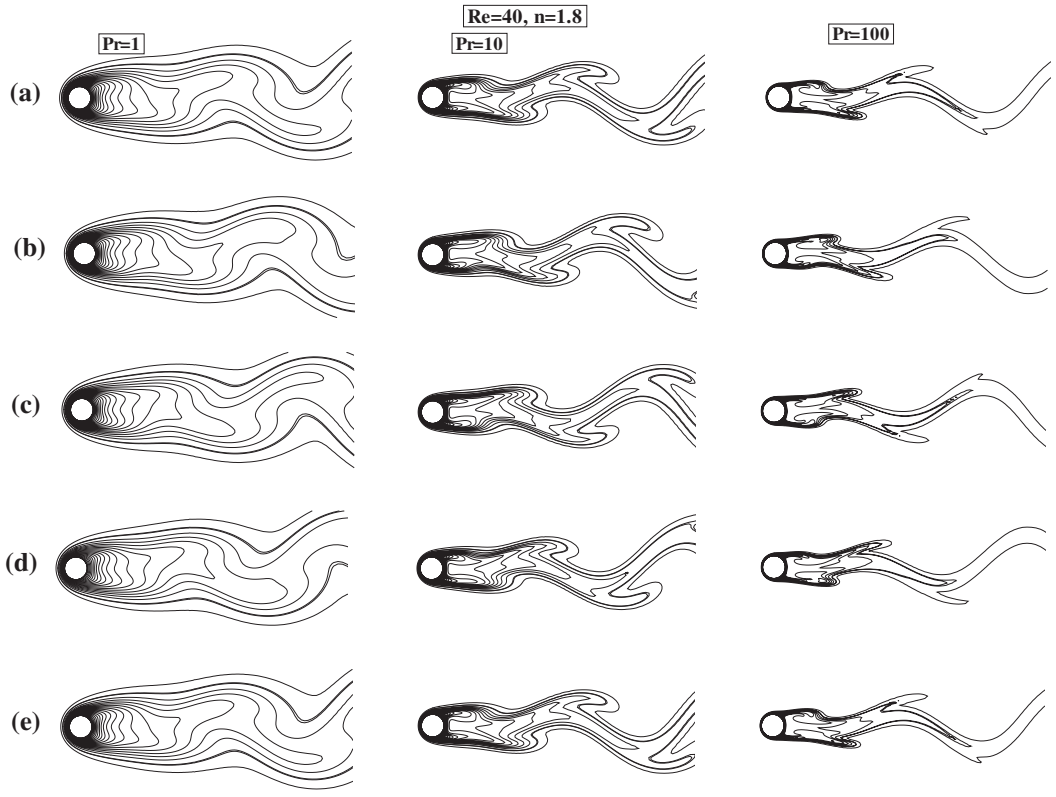

Fig. 5. Time evolution of the near wake structure of isotherm profiles for a single time period (T) at $Re = 40$ and $Pr = 1$, 10 and 100 and for power-law index $n = 1.8$ for a cylinder in cross-flow at time: (a) $t = 0$, (b) $t = T/4$, (c) $t = T/2$, (d) $t = 3T/4$ and (e) $t = T$.

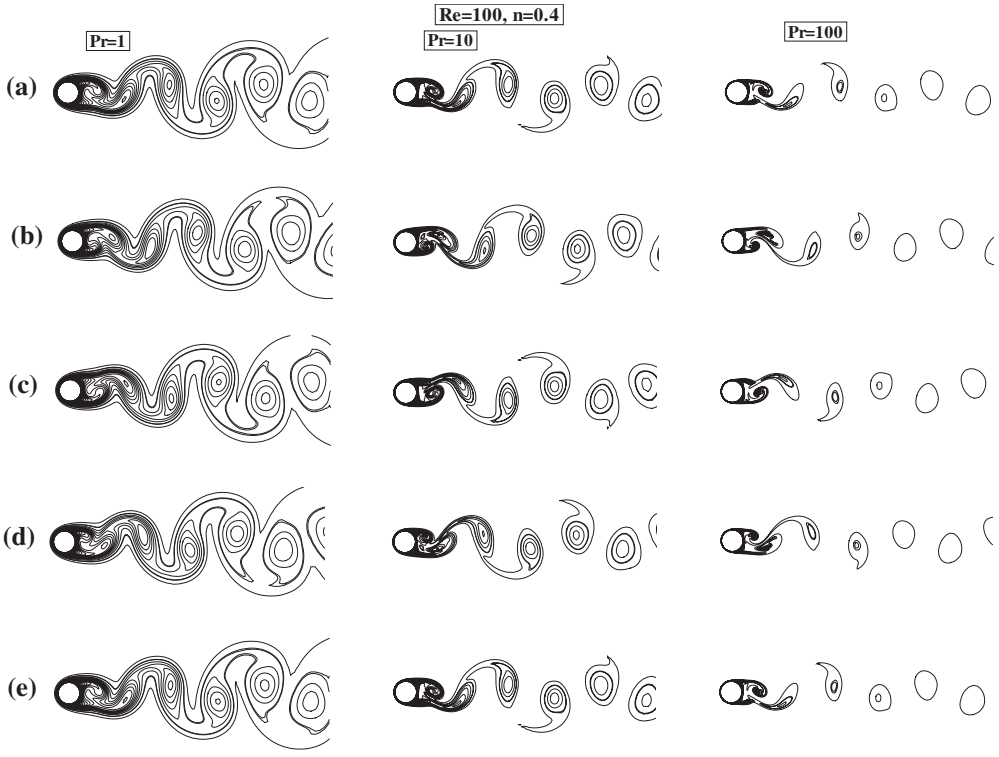

Fig. 6. Time evolution of the near wake structure of Isotherm profiles for a single time period (T) at $Re = 100$ and $Pr = 1$, 10 and 100 and for power-law index $n = 0.4$ for a cylinder in cross-flow at time: (a) $t = 0$, (b) $t = T/4$, (c) $t = T/2$, (d) $t = 3T/4$ and (e) t=T.

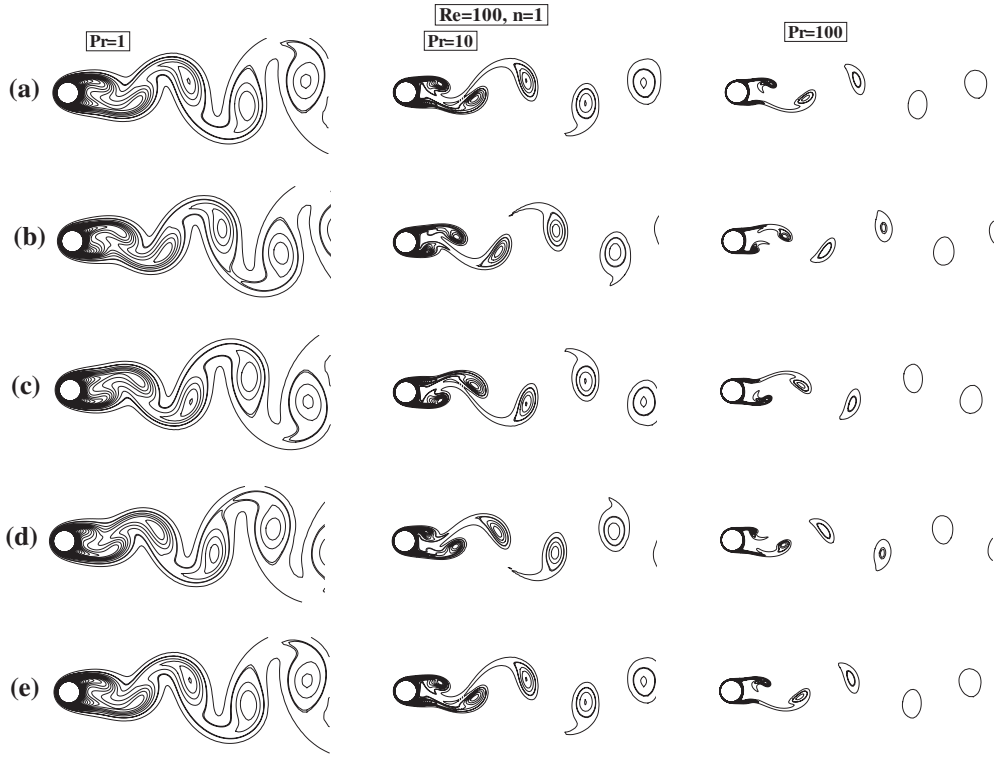

Fig. 7. Time evolution of the near wake structure of isotherm profiles for a single time period (T) at $Re = 100$ and $Pr = 1$, 10 and 100 and for power-law index $n = 1$ for a cylinder in cross-flow at time: (a) $t = 0$, (b) $t = T/4$, (c) $t = T/2$, (d) $t = 3T/4$ and (e) $t = T$.

average Nusselt number, $Nu = 5.153$ at $Re = 100$ is remarkably close to that reported by Eckert and Soehngen [40]; the two values differ only by 2%. Similarly, one of the most widely used correlation for heat transfer from a cylinder to Newtonian fluids encompassing a wide range of Prandtl number (Pr) values is that of Whitaker [41], as given below:

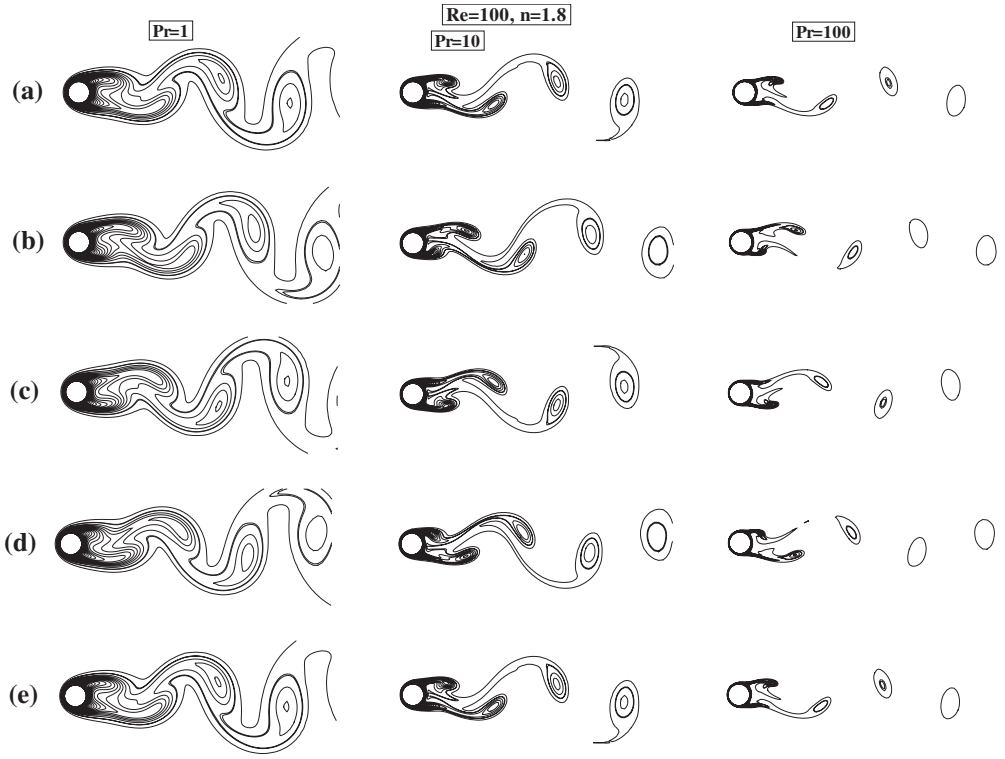

Fig. 8. Time evolution of the near wake structure of isotherm profiles for a single time period (T) at $Re = 100$ and $Pr = 1$, 10 and 100 and for power-law index $n = 1.8$ for a cylinder in cross-flow at time: (a) $t = 0$, (b) $t = T/4$, (c) $t = T/2$, (d) $t = 3T/4$ and (e) $t = T$.

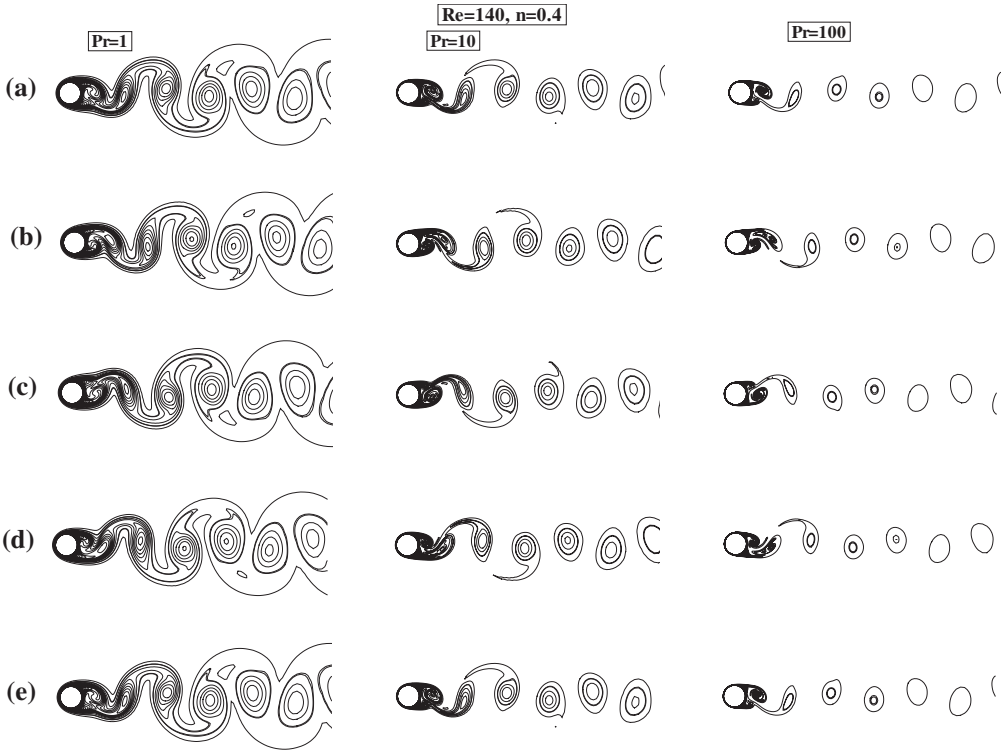

Fig. 9. Time evolution of the near wake structure of Isotherm profiles for a single time period (T) at $Re = 140$ and $Pr = 1$, 10 and 100 and for power-law index $n = 0.4$ for a cylinder in cross-flow at time: (a) $t = 0$, (b) $t = T/4$, (c) $t = T/2$, (d) $t = 3T/4$ and (e) $t = T$.

$$Nu = (0.4Re^{1/2} + 0.06Re^{2/3})Pr^{0.4}(\mu_b/\mu_o)^{0.25} \quad (16)$$

Eq. (16) was stated to correlate bulk of the literature data with an average accuracy of ±25%. Since the maximum value of $\Delta T = 2$–3 K is used in the present study the viscosity correction factor $(\mu_b/\mu_o)^{0.25} \approx 1$ and the resulting values of the mean Nusselt number are listed in Table 2. For air, the present value of the average Nusselt number (Nu) differs by about 10% from that predicted by Eq. (16).

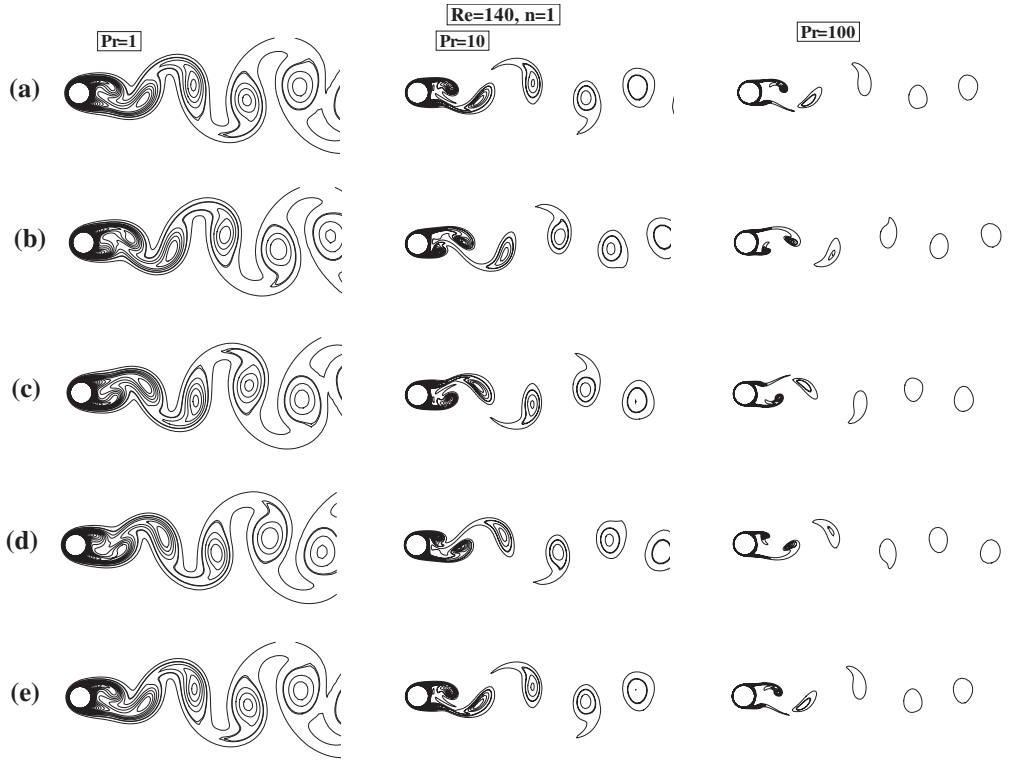

Fig. 10. Time evolution of the near wake structure of isotherm profiles for a single time period (T) at $Re = 140$ and $Pr = 1$, 10 and 100 and for power-law index $n = 1$ for a cylinder in cross-flow at time: (a) $t = 0$, (b) $t = T/4$, (c) $t = T/2$, (d) $t = 3T/4$ and (e) $t = T$.

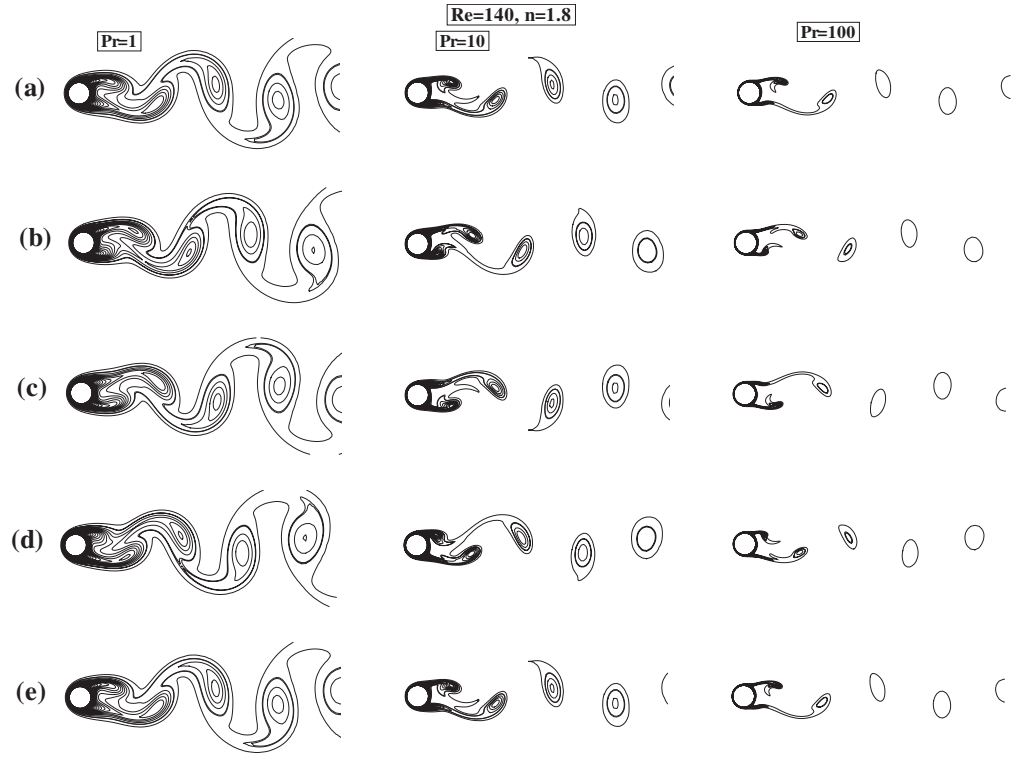

Fig. 11. Time evolution of the near wake structure of Isotherm profiles for a single time period (T) at $Re = 140$ and $Pr = 1$, 10 and 100 and for power-law index $n = 1.8$ for a cylinder in cross-flow at time: (a) $t = 0$, (b) $t = T/4$, (c) $t = T/2$, (d) $t = 3T/4$ and (e) $t = T$.

Similarly, for the higher values of Prandtl number ($Pr = 10$, 50 and 100), the present values deviate by no more than 10% from the experimental values. This order of deviation is well within the error band of Eq. (16). Such a close correspondence between the present

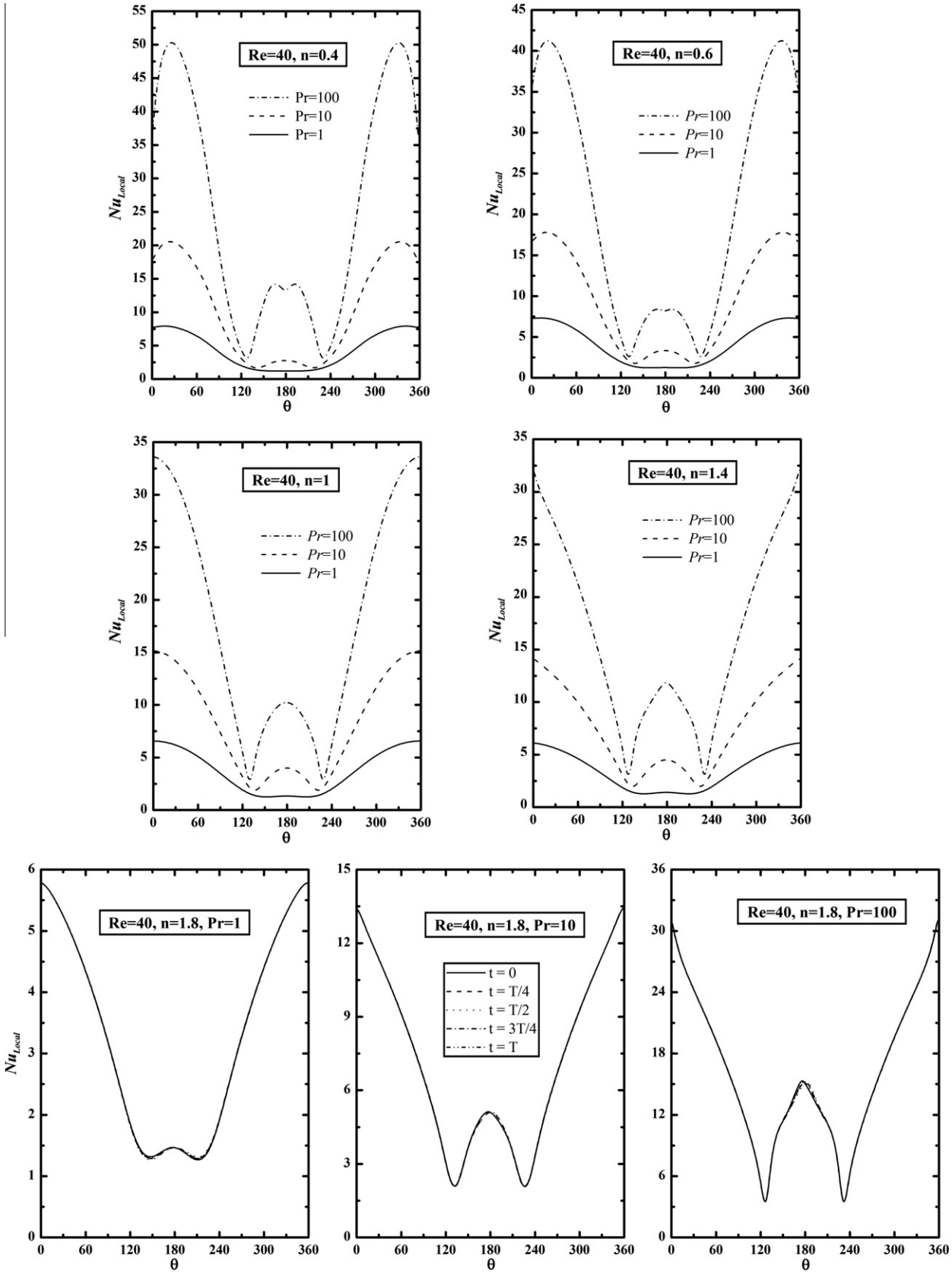

Fig. 12. Time evolution of the variation of the local Nusselt number on the surface of the cylinder in a single time period (T) for different values of power-law index (n) and Prandtl number (Pr) at Reynolds number, $Re = 40$ at time: (a) $t = 0$, (b) $t = T/4$, (c) $t = T/2$, (d) $t = 3T/4$ and (e) $t = T$.

and experimental results over a 100-fold variation in Prandtl number (Pr) inspires confidence in the new results for power-law fluids presented herein. In addition to the aforementioned benchmarking of the global characteristics, Fig. 2 shows a comparison between the

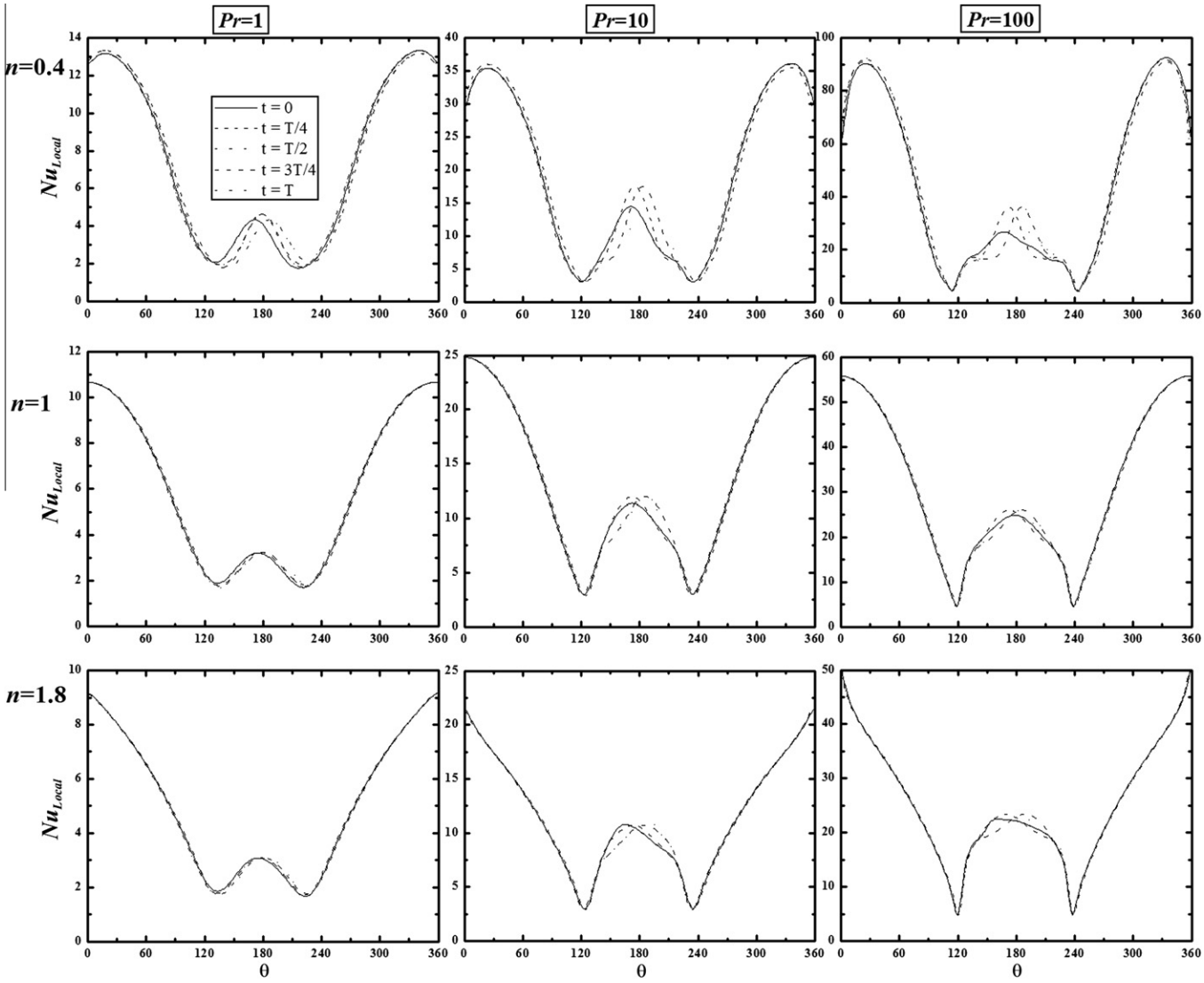

Fig. 13. Time evolution of the variation of the local Nusselt number on the surface of the cylinder in a single time period (T) for different values of power-law index (n) and Prandtl number (Pr) at Reynolds number, $Re = 100$ at time: (a) $t = 0$, (b) $t = T/4$, (c) $t = T/2$, (d) $t = 3T/4$ and (e) $t = T$.

present values of the non-dimensional surface pressure coefficient with the experimental results available in the literature [42] at $Re = 107$. The correspondence is seen to be good. Finally, Fig. 3 contrasts the present predictions of the local Nusselt number at $Re = 120$ and $Pr = 0.7$ with the experimental results of Eckert and Soehngen [40]. Once again the match is seen to be good. The detailed comparisons shown in Figs. 2 and 3 lend further support to the reliability of the new results reported herein. In summary, it is appropriate to conclude that the correspondence seen in Tables 1 and 2, and in Figs. 2 and 3 is regarded to be satisfactory and acceptable, and the present results are believed to be reliable to within ±3–4%.

6.2. Heat transfer results

Some physical insights into the nature of heat transfer can be gained by examining the isotherm (constant temperature) contours close to the surface of the cylinder and local Nusselt number variation on the surface of the cylinder.

6.2.1. Instantaneous isotherm profiles

Representative plots showing the dependence of the instantaneous isotherm patterns in the vicinity of the cylinder on the Reynolds number (Re), Prandtl number (Pr) and power-law index (n) are presented in Figs. 4–11. These figures show the periodic behavior of isotherm patterns in a time period (T) for a range of values of the Reynolds number (Re) and power-law index (n). For a fixed value of the Reynolds number (Re), as the fluid behavior changes from Newtonian ($n = 1$) to shear-thickening ($n > 1$), the isotherms become somewhat elongated and wide. The change in the liquid behavior from Newtonian ($n = 1$) to shear-thinning ($n < 1$) shows the opposite influence on the isotherm patterns. As seen in our recent study [37], the flow is expected to be steady for power-law index of $n < 1.4$ at Reynolds number of $Re = 40$ and no vortex shedding is expected to occur under these conditions. Similarly, no vortex shedding occurred in shear-thinning ($n < 1$) fluids at $Re = 40$. For Reynolds number ($Re = 40$), the isotherm lines are symmetric for power-law index of $n \leqslant 1.4$ whereas for highly shear-thickening fluids ($n = 1.8$) asymmetry is observed. It is seen that the front surface has the maximum clustering of the constant temperature lines which indicate high temperature gradients and thus high values of the local Nusselt number in this region, as compared to the other parts of the cylinder for lower value of the Prandtl number ($Pr = 1$). For a fixed value of the Reynolds number (Re), this clustering of isotherms near the rear surface of the cylinder intensifies with the increasing value of the Prandtl number (Pr).

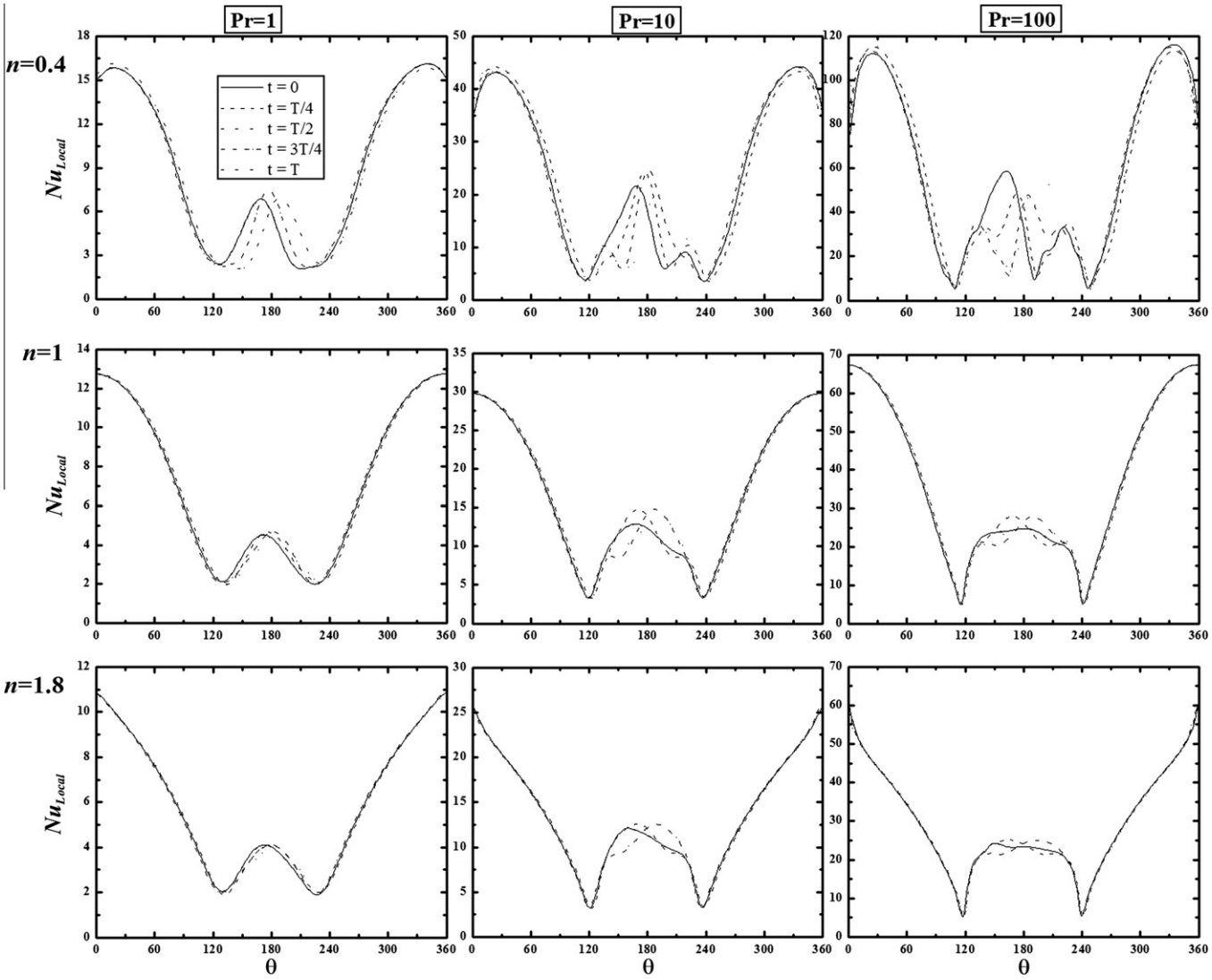

Fig. 14. Time evolution of the variation of the local Nusselt number on the surface of the cylinder in a single time period (T) for different values of power-law index (n) and Prandtl number (Pr) at Reynolds number, Re = 140 at time: (a) t = 0, (b) t = T/4, (c) t = T/2, (d) t = 3T/4 and (e) t = T.

This is, in part, due to the gradual thinning of the thermal boundary layer. The time-dependence of isotherm structures has been studied within a time period (T). For Reynolds number above 50, isotherm patterns show a constant periodic behavior. This behavior repeats again and again after each time-period. The instantaneous patterns seen in Figs. 4–11 for both shear-thinning ($n < 1$) and shear-thickening ($n > 1$) power-law fluids are qualitatively similar to that in Newtonian ($n = 1$) fluids. For instance, two (primary and secondary) closed vortices are formed in the rear of the cylinder at low Reynolds numbers. However, at high Reynolds and/or Prandtl numbers, only one closed vortex is seen in the rear of the cylinder. Irrespective of the type of fluid behaviour, the time cycle repeats in the same manner as in the Newtonian fluids. For Reynolds number (Re) values above 50, wavering motion of the layers in a time period (T) is observed in the downstream region of the cylinder. As these layers continue to move downstream, the downstream tip of each layer finally breaks off from its upstream main body. These figures also show that the neck of the layer connecting its downstream tip with the main body attached to the cylinder surface is stretched and lifted upward or downward depending on the time interval. After bending, stretching and thinning of the neck, finally the neck dislodges itself. This wave-like motion shows a regular cyclic pattern and the cycle repeats over and over again. The trends seen above are qualitatively consistent with that reported in the literature for Newtonian fluids [13–15].

6.2.2. Time evolution of the local nusselt number (Nu_{Local}) profile on the surface of cylinder

Representative instantaneous variation of the time evolution of the local Nusselt number (Nu_{Local}) over the surface of the cylinder is shown in Figs. 12–14 for a range of values of the Reynolds number (Re), Prandtl number (Pr) and flow behavior index (n). The dependence of instantaneous local Nusselt number (Nu_{Local}) profiles on the Reynolds number (Re), power-law index (n) and Prandtl number (Pr) is qualitatively similar to that reported for local Nusselt number in the steady regime [20,22,29]. For instance, for fixed values of the Reynolds number (Re), power-law index (n) and Prandtl number (Pr), the local Nusselt number (Nu_{Local}) is seen to decrease from its maximum value at the front stagnation point ($\theta = 0^o$) along the surface toward the rear of the cylinder. The maximum and minimum values of the instantaneous local Nusselt number (Nu_{Local}) occur at locations other than front ($\theta = 0^o$) and

rear ($\theta = 180^o$) stagnation points (measured from the front stagnation point). Two distinct peaks are seen under these conditions. The minimum value of the local Nusselt number (Nu_{Local}) occurs at the point of separation ($\theta = \theta_s < 180^o$) and beyond $\theta > \theta_s$, it shows some recovery up to the rear stagnation point ($\theta = 180^o$). This is clearly due to the recirculation of fluid in the rear of the cylinder. The value of the Nusselt number at the front stagnation point, $Nu(0)$ changes very little with the intervals of time step in a time period (T). On the other hand, the local Nusselt number (Nu_{Local}) in the vicinity of the rear stagnation point changes very rapidly within a time period (T). This change is suppressed with the increasing value of power-law index (n), for fixed values of Reynolds (Re) and Prandtl (Pr) numbers. Thus, the rapid fluctuations in the local Nusselt number (Nu_{Local}) are suppressed as the fluid behavior changed from shear-thickening ($n > 1$) to Newtonian ($n = 1$) and then to the shear-thinning ($n < 1$) fluids. This indicates the thinning of the boundary layer as outside the boundary layer a power-law fluid ($n < 1$) will exhibit enormously large viscosity which suppresses the rapid fluctuations. For fixed values of Prandtl number (Pr) and the flow behavior index (n), this variation increases with an increasing value of the Reynolds number (Re).

6.2.3. Average Nusselt number

In this section, the role of the flow behavior index (n), the Reynolds number (Re) and Prandtl number (Pr) on the time-averaged surface Nusselt number is discussed. Fig. 15 and Table 3 illustrate the influence of the Reynolds number (Re), Prandtl number (Pr) and flow behavior index (n) on the time-averaged Nusselt number (Nu) over the range of conditions studied herein. Generally speaking, the dependence of average Nusselt number (Nu) on the Reynolds number (Re), power-law index (n) and Prandtl number (Pr) is

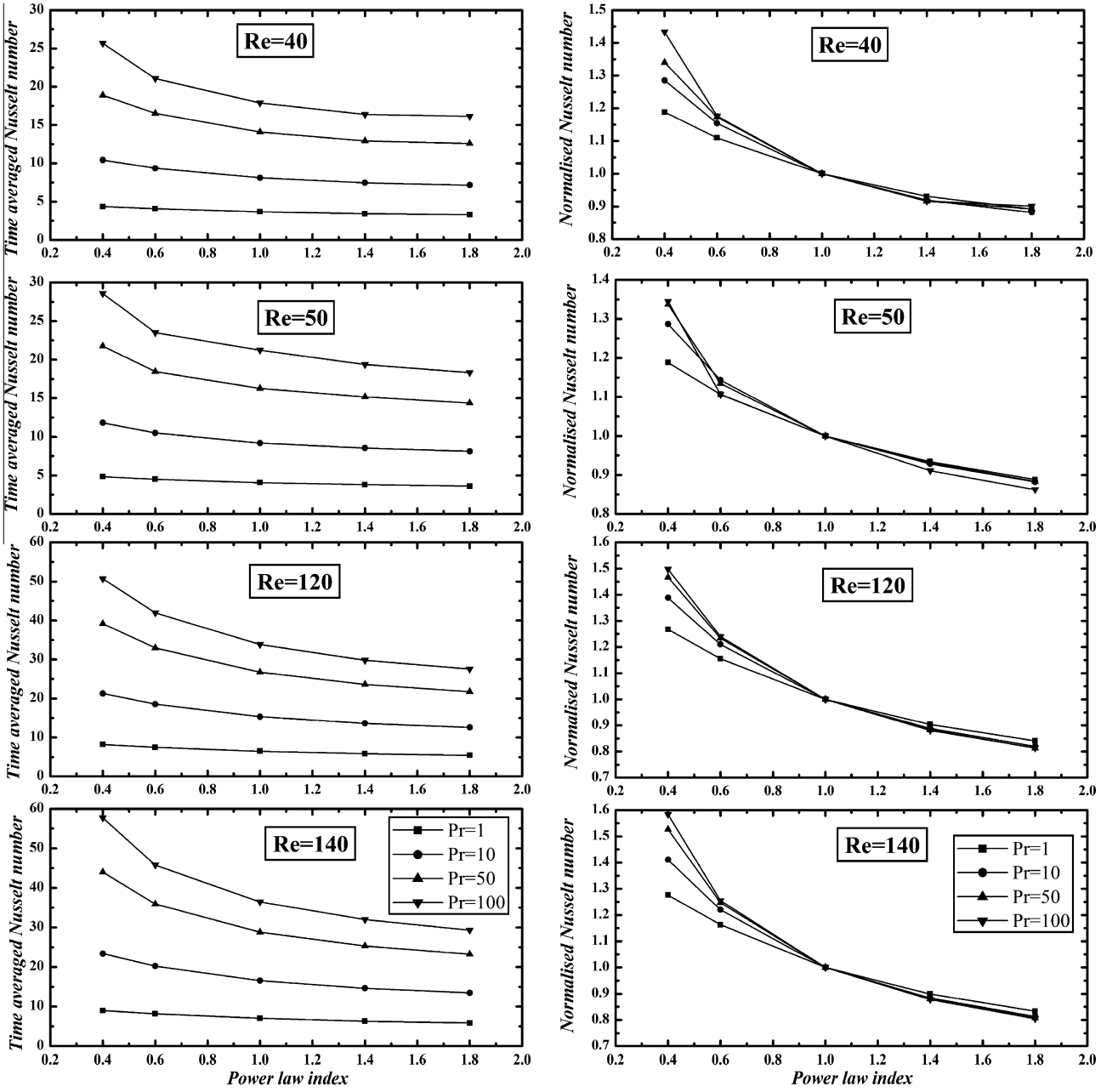

Fig. 15. Variation of surface averaged Nusselt number (Nu) with Reynolds number (Re), power-law index (n) and Prandtl number (Pr).

qualitatively similar to that seen in the steady flow regime [20,22,29]. For instance, the average Nusselt number (Nu) shows an increase with the increasing value of Reynolds number (Re) and/or Prandtl number (Pr) and/or both, irrespective of the fluid behaviour. For fixed values of the parameters (Re, Pr), the average Nusselt number (Nu) increases as the fluid behavior changes from Newtonian ($n = 1$) to shear-thinning ($n < 1$); however, the opposite effect is seen in shear-thickening ($n > 1$) fluids. This suggests that shear-thinning ($n < 1$) fluid behavior promotes heat transfer due to lower effective viscosity, and as expected, shear-thickening ($n > 1$) impedes heat transfer. Over the ranges of power-law index (n) and Reynolds number (Re), an increase in the value of Prandtl number (Pr) from 1 to 100 increases the time-averaged Nusselt number (Nu) by 5–6 folds which suggests that the time averaged Nusselt number scales with Prandtl number as $Nu \alpha Pr^{0.35}$, which is consistent with the classical (1/3) dependence and is only slightly less than the value of 0.4 in Eq. (16). The increase in the time-averaged Nusselt number (Nu) is relatively small in shear-thickening fluids ($n > 1$) compared to that in shear-thinning ($n < 1$) fluids. This is in part due to the higher effective viscosity of a shear-thickening fluid than that of a shear-thinning fluid under otherwise identical conditions.

In order to isolate the role of power-law index (n), the time-averaged Nusselt number values are normalized with respect to the corresponding Newtonian values, at the same values of Reynolds and Prandtl numbers, as follows:

$$Nu^N = \frac{Nu(n, Re, Pr)}{Nu(n = 1, Re, Pr)} \tag{17}$$

Fig. 15 also illustrates the effect of power-law index (n) on the normalized time-averaged Nusselt number (Nu^N) over the ranges of conditions studied herein. Thus, the value of normalized time-averaged Nusselt number is $Nu^N > 1$ for shear-thinning ($n < 1$) fluids thereby suggesting enhancement of up to about 40–50% and $Nu^N < 1$ for shear-thickening fluids ($n > 1$) thereby suggesting deterioration ($\sim$10–12%) in heat transfer. The influence of the power-law index (n) is seen to be stronger in shear-thinning ($n < 1$) fluids than that in shear-thickening ($n > 1$) fluids, under otherwise identical conditions, as also seen for drag coefficients [37]. This augmentation in heat transfer in shear-thinning fluids can thus be attributed to the lowering of effective viscosity.

Finally, before leaving this section, it is useful to emphasize here that both the flow and temperature fields in the vicinity of the cylinder are determined by a complex interplay between the viscous, inertial, and pressure forces prevailing in the fluid. These forces, in turn, show different scaling with respect to the power-law index, velocity and the characteristic linear dimension. For instance, the viscous forces scale as $\sim U_0^n$ whereas the inertial forces scale as U_0^2. Now, for a fixed value of velocity (U_0), the inertial force does not change, but the viscous force can decrease or increase depending upon the value of the power-law index (n). Conversely, for a given fluid, with a gradual increase in the fluid velocity, the viscous term will diminish for a shear-thinning ($n < 1$) fluid whereas it will grow in a shear-thickening ($n > 1$) fluid. Therefore, some of the trends seen in the preceding sections are due to such complex interactions.

7. Concluding remarks

Extensive numerical results on the rate of heat transfer from a cylinder to power-law fluids in the time dependent flow regime have been studied over wide ranges of conditions as: Reynolds number ($40 \leqslant Re \leqslant 140$); Prandtl number ($1 \leqslant Pr \leqslant 100$) and power-law index ($0.4 \leqslant n \leqslant 1.8$). The effects of the dimensionless parameters (Re, n, Pr) on isotherm patterns, local and averaged Nusselt number as well as their evolution with time are discussed. Depending upon the value of the power-law index, fully developed periodic regime is observed beyond the transition Reynolds number. The average Nusselt number increases with Reynolds and/or Prandtl numbers, irrespective of the value of the flow behavior index. The strong dependence of the power-law index on both local and time-averaged Nusselt number is also observed. The effect of power-law index on the heat transfer characteristics is seen to be stronger in shear-thinning fluids than that compared to the shear-thickening fluids. Broadly, it is thus possible to achieve higher rates of heat transfer in shear-thinning fluids than that in

Table 3
Dependence of the (a) average Nusselt number (Nu) and (b) amplitude of the average Nusselt number (ΔNu) on Reynolds number (Re), Prandtl number (Pr) and power-law index (n).

n	Re = 40	Re = 50	Re = 100	Re = 120	Re = 140	Re=40	Re = 50	Re = 100	Re = 120	Re = 140
(a) Average Nusselt number (Nu)										
	Pr = 1					Pr = 10				
0.4	4.3674	4.8334	7.3376	8.1964	8.9727	10.4309	11.8193	19.0500	21.2759	23.3940
0.6	4.0775	4.5029	6.7067	7.4736	8.1762	9.3639	10.5013	16.6890	18.5460	20.2373
1	3.6755	4.0686	5.8604	6.4683	7.0316	8.1159	9.1848	13.9415	15.3302	16.5843
1.4	3.4216	3.7994	5.3319	5.8466	6.3222	7.4602	8.5288	12.4590	13.6180	14.6559
1.8	3.2771	3.6139	4.9816	5.4377	5.8579	7.1561	8.1033	11.5485	12.5732	13.4855
	Pr = 50					Pr = 100				
0.4	18.8923	21.7542	34.9458	39.1836	43.9816	25.6641	28.5799	44.9473	50.6768	57.7266
0.6	16.5330	18.4603	29.7920	32.9430	35.9163	21.0598	23.5016	38.0174	41.9475	45.7478
1	14.0989	16.2746	24.3820	26.7194	28.8155	17.9052	21.2464	30.9006	33.8433	36.4659
1.4	12.9173	15.1618	21.6691	23.5973	25.3298	16.4078	19.3576	27.4000	29.8203	31.9952
1.8	12.5812	14.3842	20.0498	21.7401	23.2540	16.1327	18.3244	25.3239	27.5619	29.3403
(b) Amplitude of the average Nusselt number (ΔNu)										
0.4	–	0.00007	0.0131	0.0354	0.0661	–	–	0.1603	0.3515	0.4954
0.6	–	–	0.0051	0.0143	0.0291	–	–	0.0577	0.1364	0.2435
1	–	0.00008	0.0018	0.0044	0.0097	–	–	0.0246	0.0457	0.0729
1.4	–	0.00016	0.0011	0.0019	0.0039	–	0.00018	0.0162	0.0272	0.0394
1.8	0.00019	0.00031	0.0010	0.0012	0.0020	0.00020	0.00042	0.0125	0.0199	0.0284
	Pr = 50					Pr = 100				
0.4	–	–	0.2437	0.5013	0.7270	–	–	0.2442	0.5611	1.1698
0.6	–	–	0.0704	0.1606	0.2639	–	–	0.0678	0.1448	0.2936
1	–	–	0.0273	0.0437	0.0616	–	–	0.0241	0.0369	0.0482
1.4	–	0.00096	0.0204	0.0255	0.0319	–	0.00116	0.0157	0.0200	0.0227
1.8	0.00028	0.00138	0.0156	0.0197	0.0224	0.00044	0.00212	0.0129	0.0145	0.0155

Newtonian fluids otherwise under identical conditions. It needs to be re-iterated here that the results reported herein are limited by the assumption of constant thermo-physical properties (hence small ΔT) and hopefully, future studies in this area will endeavor to address this issue as well as other such as the role of buoyancy on the overall rate of heat transfer in this flow.

References

[1] M.M. Zdravkovich, Flow Around Circular Cylinders, Fundamentals, vol. 1, New York, Oxford University Press, 1997.
[2] M.M. Zdravkovich, Flow Around Circular Cylinders, Applications, vol. 2, New York, Oxford University Press, 1997.
[3] V.T. Morgan, The overall convective heat transfer from smooth circular cylinders, Adv. Heat Transfer 11 (1975) 199–264.
[4] R.P. Chhabra, J.F. Richardson, Non-Newtonian Flow and Applied Rheology: Engineering Applications, second ed., Butterworth-Heinemann, Oxford, 2008.
[5] R.P. Chhabra, Bubbles, Drops and Particles in Non-Newtonian Fluids, second ed., FL: CRC Press, Boca Raton, 2006.
[6] C. Norberg, An experimental investigation of the flow around a circular cylinder: influence of aspect ratio, J. Fluid Mech. 258 (1994) 287–316.
[7] P. Le Gal, A. Nadim, M.C. Thompson, Hysteresis in the forced Stuart–Landau equation: application to vortex shedding from an oscillating cylinder, J. Fluids Struct. 15 (2001) 445–457.
[8] D. Barkley, R.D. Henderson, Three-dimensional Floquet stability analysis of the wake of a circular cylinder, J. Fluid Mech. 322 (1996) 215–241.
[9] B.M. Sumer, J. Fredsoe, Hydrodynamics Around Cylindrical Structures, World Scientific, Singapore, 2006.
[10] R.A. Ahmad, Steady state numerical solution of the Navier–Stokes and energy equations around a horizontal cylinder at moderate Reynolds numbers from 100 to 500, Heat Transfer Eng. 17 (1996) 31–81.
[11] R.P. Bharti, R.P. Chhabra, V. Eswaran, A numerical study of the steady forced convection heat transfer from an unconfined circular cylinder, Heat Mass Transfer 43 (2007) 639–648.
[12] M.W. Chang, B.A. Finlayson, Heat transfer in flow past cylinders at Re < 150 – Part I. Calculations for constant fluid properties, Numer. Heat Transfer 12 (1987) 179–195.
[13] G.E. Karniadakis, Numerical simulation of forced convection heat transfer from a cylinder in cross flow, Int. J. Heat Mass Transfer 31 (1988) 107–118.
[14] C.-H. Cheng, J.-L. Hong, A. Win, Numerical prediction of lock-on effect on convective heat transfer from a transversely oscillating circular cylinder, Int. J. Heat Mass Transfer 40 (1997) 1825–1834.
[15] F.M. Mahfouz, H.M. Badr, Forced convection from a rotationally oscillating cylinder placed in a uniform stream, Int. J. Heat Mass Transfer 43 (2000) 3093–3104.
[16] C.F. Lange, F. Durst, M. Breuer, Momentum and heat transfer from cylinder in laminar cross-flow at $10^{-4} \leqslant Re \leqslant 200$, Int. J. Heat Mass Transfer 41 (1998) 3409–3430.
[17] L. Baranyi, Computation of unsteady momentum and heat transfer from a fixed circular cylinder in laminar flow, J. Comput. Appl. Mech 4 (2003) 13–25.
[18] S.J.D. D'Alessio, J.P. Pascal, Steady flow of a power-law fluid past a cylinder, Acta Mech. 117 (1996) 87–100.
[19] R.P. Chhabra, A.A. Soares, J.M. Ferreira, Steady non-Newtonian flow past a circular cylinder: a numerical study, Acta Mech. 172 (2004) 1–16.
[20] A.A. Soares, J.M. Ferreira, R.P. Chhabra, Flow and forced convection heat transfer in cross flow of non-Newtonian fluids over a circular cylinder, Ind. Eng. Chem. Res. 44 (2005) 5815–5827.
[21] R.P. Bharti, R.P. Chhabra, V. Eswaran, Steady flow of power-law fluids across a circular cylinder, Can. J. Chem. Eng. 84 (2006) 406–421.
[22] R.P. Bharti, R.P. Chhabra, V. Eswaran, Steady forced convection heat transfer from a heated circular cylinder to power-law fluids, Int. J. Heat Mass Transfer 50 (2007) 977–990.
[23] P. Sivakumar, R.P. Bharti, R.P. Chhabra, Effect of power-law index on critical parameters for power-law flow across an unconfined circular cylinder, Chem. Eng. Sci. 61 (2006) 6035–6046.
[24] A.A. Soares, J. Anacleto, L. Caramelo, J.M. Ferreria, R.P. Chhabra, Mixed convection from a circular cylinder to power-law fluids, Ind. Eng. Chem. Res. 48 (2009) 8219–8231.
[25] A.T. Srinivas, R.P. Bharti, R.P. Chhabra, Mixed convection heat transfer from a cylinder in power-law fluids: effect of aiding buoyancy, Ind. Eng. Chem. Res. 48 (2009) 9735–9754.
[26] P. Sivakumar, R.P. Bharti, R.P. Chhabra, Steady flow of power-law fluids across an unconfined elliptical cylinder, Chem. Eng. Sci. 62 (2007) 1682–1702.
[27] R.P. Bharti, P. Sivakumar, R.P. Chhabra, Forced convection heat transfer from an elliptical cylinder to power-law fluids, Int. J. Heat Mass Transfer 51 (2008) 1838–1853.
[28] R.P. Bharti, R.P. Chhabra, V. Eswaran, Two-dimensional steady Poiseuille flow of power-law fluids across a circular cylinder in a plane confined channel: wall effects and drag coefficients, Ind. Eng. Chem. Res. 46 (2007) 3820–3840.
[29] R.P. Bharti, R.P. Chhabra, V. Eswaran, Effect of blockage on heat transfer from a cylinder to power-law liquids, Chem. Eng. Sci. 62 (2007) 4729–4741.
[30] R.C. Patil, R.P. Bharti, R.P. Chhabra, Steady flow of power-law fluids over a pair of cylinders in tandem arrangement, Ind. Eng. Chem. Res. 47 (2008) 1660–1683.
[31] R.C. Patil, R.P. Bharti, R.P. Chhabra, Forced convection heat transfer in power-law liquids from a pair of cylinders in tandem arrangement, Ind. Eng. Chem. Res. 47 (2008) 9141–9164.
[32] A.K. Dhiman, R.P. Chhabra, V. Eswaran, Heat transfer to power law fluids from a heated square cylinder, Numer. Heat Transfer 52 (2007) 185–201.
[33] A.K. Dhiman, N. Anjaiah, R.P. Chhabra, V. Eswaran, Mixed convection from a heated square cylinder to Newtonian and power-law fluids, J. Fluids Eng. 129 (2007) 506–513.
[34] A.K. Dhiman, R.P. Chhabra, V. Eswaran, Steady mixed convection from a confined square cylinder, Int. Commun. Heat Mass Transfer 35 (2008) 47–55.
[35] A.K. Sahu, R.P. Chhabra, V. Eswaran, Effects of Reynolds and Prandtl numbers on heat transfer from a square cylinder in the unsteady flow regime, Int. J. Heat Mass Transfer 52 (2009) 839–850.
[36] A.K. Sahu, R.P. Chhabra, V. Eswaran, Forced convection heat transfer from a heated square cylinder to power-law fluids in the unsteady flow regime, Numer. Heat Transfer, Part A. 56 (2009) 109–131.
[37] V.K. Patnana, R.P. Bharti, R.P. Chhabra, Two-dimensional unsteady flow of power-law fluids over a cylinder, Chem. Eng. Sci. 64 (2009) 2978–2999.
[38] R.B. Bird, W.E. Stewart, E.N. Lightfoot, Transport Phenomena, second ed., John Wiley & Sons, Inc, New York, 2002.
[39] R.P. Chhabra, Heat and mass transfer in rheologically complex systems, in: D. Siginer, D. De Kee, R.P. Chhabra (Eds.), Advances in the Rheology and Flow of Non-Newtonian Fluids, Elsevier, Amsterdam, 1999 (Chapter 39).
[40] E.R.G. Eckert, E. Soehngen, Distribution of heat transfer coefficients around circular cylinders in cross flow at Reynolds numbers from 20 to 500, Trans. ASME 74 (1952) 343–347.
[41] S. Whitaker, Forced convection heat transfer correlations for flow in pipes, past flat plates, single cylinders, single sphere and for flow in packed beds and tube bundles, AIChE J. 18 (1972) 361–371.
[42] F. Homann, Influence of higher viscosity on flow around cylinder, Forsch. Gebiete Ingenieur 17 (1936) 1–10.